

A COMPARISON OF CONTROL ARCHITECTURES FOR ATOMIC FORCE MICROSCOPES

J. A. Butterworth, L. Y. Pao, and D. Y. Abramovitch

ABSTRACT

We evaluate the performance of two control architectures applied to atomic force microscopes (AFM). Feedback-only control is a natural solution and has been applied widely. Expanding on that, combining feedback controllers with plant-injection feedforward filters has been shown to greatly improve tracking performance in AFMs. Alternatively, performance can also be improved by the use of a closed-loop-injection feedforward filter applied to the reference input before it enters the feedback loop. In this paper, we compare the plant-injection architecture with the closed-loop-injection architecture when used in controlling AFMs. In particular, we provide experimental results demonstrating the closed-loop-injection architecture yields better tracking performance of a raster scan.

Key Words: Atomic force microscope, feedforward control.

I. INTRODUCTION

Several research groups have investigated improving upon the performance of feedback-only AFM control by combining it with a feedforward filter. In this Brief Paper, which is a summary and extension of a previous tutorial paper [1], we discuss two distinct combined feedforward/feedback architectures that have been developed and have recently appeared in the AFM

literature: the plant-injection and closed-loop-injection architectures.

When using the feedforward plant-injection (FFPI) architecture, F_P in Fig. 1 is designed to perform as the feedforward filter while F_{CL} is set depending on the type of controller used for F_P . Most often F_{CL} is the identity or a delay function in the FFPI architecture. Some examples of applying the plant-injection architecture to AFMs in the literature include [2–6]. When using the feedforward *closed-loop-injection* (FFCLI) architecture, F_P in Fig. 1 is set to zero and the feedforward filter F_{CL} acts on the reference signal ahead of the closed-loop system [1, 7–9].

This paper is organized as follows. More details on the plant-injection and closed-loop-injection architectures are presented in Sections II and III, respectively. In Section IV, we present experimental results comparing the architectures as applied to the x -axis of an AFM. These results show that the closed-loop-injection outperforms the plant-injection architecture. We then draw conclusions and discuss future work for further improving the control of AFMs in Section V. As a *Brief Paper*, we will limit the feedforward discussion to include only model-inverse methods. Using H_∞ feedforward control also yields results showing that FFCLI outperforms the FFPI architecture for tracking control [1].

Manuscript received February 16, 2008; revised October 2, 2008; accepted December 10, 2008.

J. A. Butterworth is a graduate student and L. Y. Pao is a professor of Electrical and Computer Engineering at the University of Colorado at Boulder, Boulder, CO 80309, U.S.A. (e-mails: butterwo@colorado.edu; pao@colorado.edu).

D. Y. Abramovitch is a senior research engineer in the Nanotechnology Group at Agilent Laboratories, 5301 Stevens Creek Blvd., M/S: 4U-SB, Santa Clara, CA 95051, U.S.A. (e-mail: danny@agilent.com).

This work was supported in part by Agilent Technologies, Inc., the US National Science Foundation (NSF Grant CMMI-0700877), and the Miller Institute for Basic Research in Science at the University of California at Berkeley.

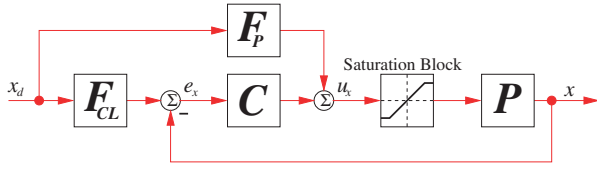


Fig. 1. A single-input single-output (SISO) block diagram of an AFM's x -direction consisting of a feedback compensator C , a plant-injection feedforward controller F_P , and a closed-loop-injection feedforward controller F_{CL} . When using the closed-loop injection architecture, F_P is set to zero. In contrast, when using the plant-injection architecture, F_{CL} is set to the identity (or a delay in the case of model-inverse control when the relative degree of the plant is greater than zero). The saturation block is representative of limitations of our actual system.

II. PLANT-INJECTION ARCHITECTURE

Recent work in AFMs has shown increases in AFM performance when feedback controllers are combined with a feedforward controller in the plant-injection architecture [2–5, 10]. In general, this architecture ensures stability through the feedback controller C while the feedforward controller F_P further increases tracking performance, disturbance rejection, and robustness to model uncertainties.

Similar to work in [11], we examine the transfer function from the desired input x_d to the output x of the FFPI system of Fig. 1. Ignoring the saturation block, and assuming F_{CL} is unity, the transfer function is

$$\left. \frac{X(z)}{X_d(z)} \right|_{FFPI} = \frac{P(z)F_P(z) + P(z)C(z)}{1 + P(z)C(z)}. \quad (1)$$

It should be clear that if the feedforward filter $F_P(z) = 0$, then (1) reduces to the common expression for the dynamics of a feedback-only closed-loop system,

$$H_{CL}(z) = \frac{P(z)C(z)}{1 + P(z)C(z)}. \quad (2)$$

When $F_P(z)$ is equal to the inverse of $P(z)$, then (1) becomes the identity and we are able to track any desired input perfectly. Of course, this assumes a perfect inverse of $P(z)$ exists and is practically implementable, and we will discuss this further in Subsection 2.1.

For convenience we drop the argument z , and define the plant dynamics P , the feedback controller C , and the feedforward controller F_P as a ratio of polynomials as in

$$P = \frac{B}{A}, \quad C = \frac{C_N}{C_D}, \quad \text{and} \quad F_P = \frac{F_{PN}}{F_{PD}}. \quad (3)$$

The subscripts N and D indicate numerator or denominator polynomials. A and B represent polynomials

defining the plant poles and zeros, respectively. Using the definitions in (3), we can further reduce (2) and (1) to

$$H_{CL} = \frac{BC_N}{AC_D + BC_N} \quad (4)$$

and

$$\left. \frac{X(z)}{X_d(z)} \right|_{FFPI} = \frac{BF_{PN}C_D + BC_NF_{PD}}{F_{PD}(AC_D + BC_N)}. \quad (5)$$

Equation (5) provides us with an overall transfer function for the FFPI architecture regardless of the design of F_P . Below, we design F_P using model-inverse techniques.

2.1 FFPI: Feedforward model-inverse control

Devasia and others have studied model-inverse methods applied in the plant-injection architecture for AFMs [2, 3, 6, 10], where C in Fig. 1 is some feedback controller and F_P is set *approximately* equal to \hat{P}^{-1} , the inverse of the plant model. Ideally, F_P is equal to \hat{P}^{-1} , or even better, F_P is equal to P^{-1} . However, often the existence of nonminimum-phase zeros in the plant force a *stable* approximate inverse to be used in place of the exact inverse. In AFMs, the plant and hence model of piezo scanners typically have nonminimum-phase zeros due to the existence of non-collocated sensing and actuation and flexible modes. Many control systems researchers, working in a myriad of application areas, have developed and used stable approximate inversions in order to implement model-inverse based control on nonminimum-phase systems; this work has been applied to both the plant-injection and closed-loop-injection architectures [3, 11–15].

Various stable approximate model-inversion techniques exist, but we focus on two simple and effective techniques: Tomizuka's popular *zero-phase-error tracking controller* (ZPETC) [14], and a cousin of the ZPETC, the comparably named *zero-magnitude-error tracking controller* (ZMETC) that has appeared in [1, 11, 13, 15]. Ultimately, the proper choice of a stable approximate model-inversion technique depends on the system on which it will be applied and how the controller will be implemented [16]. Generally, ZPETC and ZMETC offer simple and *usually* effective methods for model-inverse control [11]. When compared to ZPETC, ZMETC provides better performance results when applied to our AFM x - y stage, and as such it will be the focus of the discussion of the model-inversion technique for the duration of this paper. Later in Subsection 4.1, we will discuss the importance of magnitude tracking (rather than phase) for obtaining

high quality AFM images. As a result, the use of the *zero-magnitude-error* tracking controller is natural to our overall goals.

To design a ZMETC stable approximate model inverse of a nonminimum-phase plant, write the model of the plant dynamics as in (6), partitioning the polynomial \hat{B}_s containing the stable (invertible) zeros from the polynomial \hat{B}_u containing the unstable (noninvertible) zeros:

$$\hat{P}(z) = \frac{\hat{B}(z)}{\hat{A}(z)} = \frac{\hat{B}_s(z)\hat{B}_u(z)}{\hat{A}(z)} \quad (6)$$

The polynomial $\hat{A}(z)$ contains all the poles of the model of the plant. \hat{B}_u has the form

$$\hat{B}_u(z) = b_{un}z^n + b_{u(n-1)}z^{n-1} + \dots + b_{u0} \quad (7)$$

where n is the number of nonminimum-phase zeros. The ZMETC technique then yields a stable approximation of the inverse of the plant

$$\tilde{P}^{-1}(z) = \frac{\hat{A}(z)}{\hat{B}_s(z)\hat{B}_u^*(z)}, \quad (8)$$

where the \sim indicates an *approximate* inverse (as compared to a \wedge indicating the *model* of the plant), and $\hat{B}_u^*(z)$ is

$$\hat{B}_u^*(z) = b_{u0}z^n + b_{u1}z^{n-1} + \dots + b_{un}. \quad (9)$$

Note that the difference between (7) and (9) is the “flipping” of the coefficients. It is this action which reflects the unstable $\hat{B}_u(z)$ about $|z|=1$ into the stable $\hat{B}_u^*(z)$. Setting F_P equal to $\tilde{P}^{-1}(z)$ and F_{CL} equal to unity or a delay block (discussed further below) in Fig. 1 would constitute a model-inverse based control using the plant-injection architecture.

If the relative degree r of $P(z)$ is greater than zero, the resulting $\tilde{P}^{-1}(z)$ will be noncausal. Additional delay equal to r will have to be added in order for F_P to be implementable in a causal way:

$$F_P = \tilde{P}^{-1}(z) = \frac{z^{-r}\hat{A}(z)}{\hat{B}_s(z)\hat{B}_u^*(z)}. \quad (10)$$

If $r > 0$, then the feedforward block F_{CL} should be defined not as unity, but rather as a delay block equal to z^{-r} . Setting $F_{CL} = z^{-r}$ changes the transfer function in (1) to

$$\frac{X(z)}{X_d(z)} \Big|_{FFPI} = \frac{P(z)F_P(z) + z^{-r}P(z)C(z)}{1 + P(z)C(z)}. \quad (11)$$

If (a) there exist no nonminimum-phase zeros in the plant, (b) the model exactly matches the plant

($\hat{P}(z) = P(z)$), and (c) $r=0$, then the output of the system exactly tracks the desired input x_d and the feedback loop is not excited. If the first two conditions (a) and (b) hold and $r > 0$, then the output of the system exactly tracks the desired input x_d with a delay of r .

Returning to the discussion of FFPI, if we assume a nonminimum-phase, perfectly known plant ($\hat{P}(z) = P(z)$) with relative degree r , we can apply the above discussion on ZMETC and write (4) and (11) as

$$H_{CL} = \frac{B_{sCL}B_{uCL}}{A_{CL}} = \frac{(B_sC_N)(B_u)}{AC_D + B_sB_uC_N} \quad (12)$$

and

$$\begin{aligned} \frac{X(z)}{X_d(z)} \Big|_{FFPI} &= \frac{B_uAC_D + B_sB_uC_NB_u^*}{z^rB_u^*(AC_D + B_sB_uC_N)} \\ &= \frac{AC_D + B_sB_u^*C_N}{z^rB_u^*B_sC_N} H_{CL}. \end{aligned} \quad (13)$$

Now, if we define

$$\Psi(z) = \frac{AC_D + B_sB_u^*C_N}{AC_D + B_sB_uC_N}, \quad (14)$$

we can rewrite (13) in the compact form of (15) that will be valuable to us when we compare with the corresponding transfer function in the FFCLI architecture in Section III.

$$\frac{X(z)}{X_d(z)} \Big|_{FFPI} = \Psi(z) \frac{z^{-r}B_u}{B_u^*} \quad (15)$$

It should be clear that if all plant zeros are minimum phase, then (15) reduces to a delay block indicating perfectly delayed tracking.

III. CLOSED-LOOP-INJECTION ARCHITECTURE

When compared to plant-injection, the closed-loop-injection’s superior ability to perform under the presence of uncertainties in a disk drive application [11] provides motivation for application to AFM control. The same feedforward techniques overviewed in Section II are briefly discussed specifically for the closed-loop-injection architecture below.

In this architecture, we set F_P in Fig. 1 equal to zero and design F_{CL} accordingly. Ignoring the saturation block, we can condense a FFCLI version of Fig. 1 into a transfer function from the desired input x_d to the

output x :

$$\left. \frac{X(z)}{X_d(z)} \right|_{FFCLI} = H_{CL} F_{CL}. \quad (16)$$

If we make the assumption that a stable inverse of H_{CL} exists, we can see that setting F_{CL} equal to that stable inverse would result in perfect tracking.

Further, the feedforward filter F_{CL} functions ahead of the loop that is stabilized by the feedback controller C . In this arrangement, we expect the feedback controller C to be continually excited. This is in contrast to the plant-injection architecture where the feedback loop is not activated unless modeling errors or deficiencies in the approximate model inverse force the feedback controller to be excited.

3.1 FFCLI: Feedforward model-inverse control

The creation of a ZMETC model-inverse controller for the closed-loop-injection architecture follows very closely to the ZMETC procedure described in Subsection 2.1 for plant-injection architectures. The major difference is the use of ZMETC to create a stable approximate model inverse of the closed-loop dynamics ($H_{CL}(z)$) and setting F_{CL} in Fig. 1 equal to that approximate inverse $\tilde{H}_{CL}^{-1}(z)$. Following the technique described in Subsection 2.1, and making the assumption that the feedback controller C is stable, minimum phase, and exactly proper, we obtain an approximate stable inverse of $H_{CL}(z)$:

$$\begin{aligned} F_{CL} = \tilde{H}_{CL}^{-1} &= \frac{z^{-r} \hat{A}_{CL}}{\hat{B}_{sCL} \hat{B}_{uCL}^*} \\ &= \frac{z^{-r} (\hat{A}C_D + \hat{B}_s \hat{B}_u C_N)}{(\hat{B}_s C_N)(\hat{B}_u^*)} \end{aligned} \quad (17)$$

where (12) defines A_{CL} and B_{sCL} . For minimum phase C , B_{uCL}^* is equal to the same B_u^* from Subsection 2.1. Because C is assumed to be exactly proper, the relative degree r remains the same as before as well.

With C stable, minimum phase, and exactly proper, and further assuming the nonminimum-phase plant is known with certainty, we can use (12) and (17) to rewrite (16):

$$\begin{aligned} \left. \frac{X(z)}{X_d(z)} \right|_{FFCLI} &= \frac{(B_s C_N) B_u}{A C_D + B_s B_u C_N} \frac{z^{-r} (A C_D + B_s B_u C_N)}{(B_s C_N)(B_u^*)} \\ &= \frac{z^{-r} B_u}{B_u^*}. \end{aligned} \quad (18)$$

Comparing (18) with (15) for the FFPI architecture, we see one of the advantages of FFCLI over FFPI. In (18), the transfer function from x_d to x reduces to a transfer function with unity gain at all frequencies and possibly some phase delay. This is in contrast to (15) of the plant-injection architecture which also includes the term $\Psi(z)$ defined in (14). We will look more closely at the effect of $\Psi(z)$ in Section IV.

Like the FFPI architecture, we can see that when $H_{CL}(z)$ is minimum-phase and the model $\hat{P}(z)$ is known with certainty, (18) becomes unity or a delay block. In this case, we can expect x to perfectly track x_d (perhaps with some delay).

IV. EXPERIMENTAL RESULTS AND DISCUSSION

This section presents experimental results of a comparison of the FFPI and FFCLI architectures. First, we discuss a metric used to compare the results, then we provide experimental data showing the performance of each architecture. All laboratory work was performed on the x direction of a nPoint NPXY100A x - y piezoscanner stage, and controllers were implemented on a Texas Instruments digital signal processor. Using frequency response methods, we obtained a 4th-order discrete-time model of the stage. The model includes two nonminimum-phase zeros that challenge the performance of control designs and limit the effectiveness of the model-inverse based feedforward methods. The relative degree $r = 2$, and the sample rate for this model and all associated controllers is 25 kHz.

4.1 Performance metrics

When discussing the performance of the tracking of a raster scan in AFMs, it is important to recall the overall goal of AFMs: to create a quality image in a timely manner. But this goal requires a definition of a “quality image” when referring to an x - y raster scan. Focusing on the x direction, an ideal controller would cause the system output $x(t)$ to track the desired raster pattern $x_d(t)$ flawlessly. This suggests that a mean-square-error metric might be informative in defining the performance of a controller. However, *for imaging*, mean-square error might not give us the best measurement. This is because phase lag in the raster scan used for AFM imaging is not nearly as critical as consistently tracking the magnitude. Ultimately, this means that perfectly delayed tracking is better than imperfect timely tracking if we know the delay well. So, to identify that delay, we examine one period T of

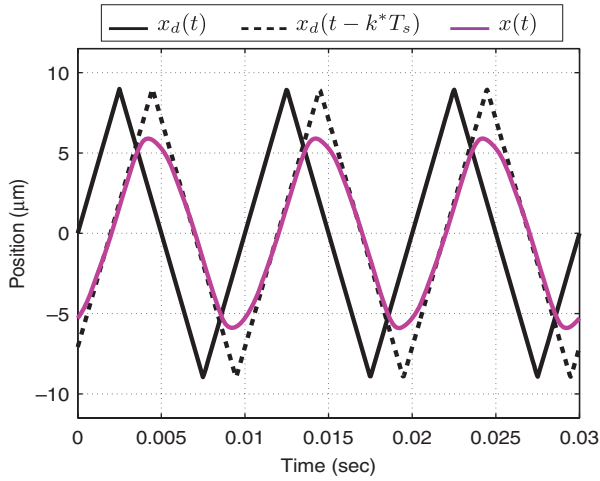


Fig. 2. Example of simulation results using PID feedback-only. Three curves appear in the figure: the $x_d(t)$ input, the $x_d(t - k^*T_s)$ used for the performance metrics $J_{e\tau}$ and $J_{m\tau}$, and the $x(t)$ output.

the raster scan after a time t_{ss} after which all transients (from initial conditions for example) have died out, and define the integer variable k^* as

$$k^* = \arg \min_k \int_{t_{ss}}^{t_{ss}+T} (x_d(t - kT_s) - x(t))^2 dt. \quad (19)$$

Here, k is also an integer and is defined on $[0, \frac{T}{T_s}]$ where $T_s = 40 \mu\text{sec}$ is the controller sample period. k^* is defined to be an integer as it represents actual implementation in a digital controller. Specifically, k^* reflects the phase lag in the system or in other words, the discrete delay. We can then use this information to define two metrics that disregard the phase lag in the system and emphasizes magnitude tracking:

$$J_{e\tau} = \int_{t_{ss}}^{t_{ss}+T} (x_d(t - k^*T_s) - x(t))^2 dt \quad (20)$$

$$J_{m\tau} = \max_{t \in [t_{ss}, t_{ss}+T]} (x_d(t - k^*T_s) - x(t))^2 \quad (21)$$

For further clarification, we provide Fig. 2 which is an example simulation of a 100 Hz raster scan input into a PID feedback-only control loop. We have chosen a simple PID feedback-only simulation as an example for its clear delineation of each line. We see the actual 100 Hz raster scan input $x_d(t)$ in solid black, and the shifted 100 Hz input $x_d(t - k^*T_s)$ in dashed black. From Fig. 2, it is clear that the PID feedback-only controller lacks the bandwidth to be able to track the 100 Hz raster scan. Images created while using this raster scan would be highly distorted at the edges.

4.2 Experimental results

In Fig. 3, we provide experimental results comparing the FFPI and FFCLI architectures. In this comparison, the exact same 5th-order H_∞ feedback controller C is used for both experiments. Although neither is perfect, the reader should notice the FFCLI architecture’s ability to track the supplied 99.2 Hz raster pattern better than the FFPI architecture. Specifically, the FFPI architecture overshoots the corners of the raster pattern. In contrast, the FFCLI architecture tracks the corners and the rest of the pattern with $J_{e\tau}$ and $J_{m\tau}$ metrics an order of magnitude less than those of FFPI.

The overshoot associated with the plant-injection architecture can be understood by looking at the frequency response of the transfer function Ψ for this particular case. In Fig. 4, we notice the variation of the magnitude and phase. This in contrast to the factor $\frac{z^{-\tau} B_u}{B_u^*}$ which would have unity magnitude for all frequencies and phase loss due to delay. In particular, the magnitude of Ψ at 99.2 Hz (the raster frequency) in Fig. 4 is 1.24 (1.86 dB) which is in the neighborhood of the overshoot magnitude shown in Fig. 3(a). From this plot, we can see that under these conditions, the FFCLI architecture will always outperform FFPI except at low frequencies (which are trivial) and *in simulation* at very high frequencies. The high-frequency rasters are not realistic for hardware comparisons because of many problems including low signal-to-noise ratio, signal saturation, vibrations inherent to the piezos and more.

V. CONCLUSIONS AND FUTURE WORK

We have compared two control architectures and have shown in detailed simulation studies [1] and here in hardware experiments that when using the exact same feedback controller, the closed-loop-injection architecture leads to more precise tracking of a raster scan than the plant-injection architecture. Beyond performance, FFCLI has some advantages over the FFPI architecture. Specifically in Subsection 3.1, we show that when using model-inverse control, the dynamics of the overall FFCLI SISO transfer function from the desired output (reference x_d) to the actual output (x) can reduce to a delay block and filter of order much lower than that of the original plant. Further, when F_P is not a perfect inverse of the true plant, the closed-loop dynamics can be excited in such a way that limit the performance of the overall system. Finally, in many systems, system identification can only be done (or is best done) in closed-loop which indicates the closed-loop-injection architecture as a natural choice.

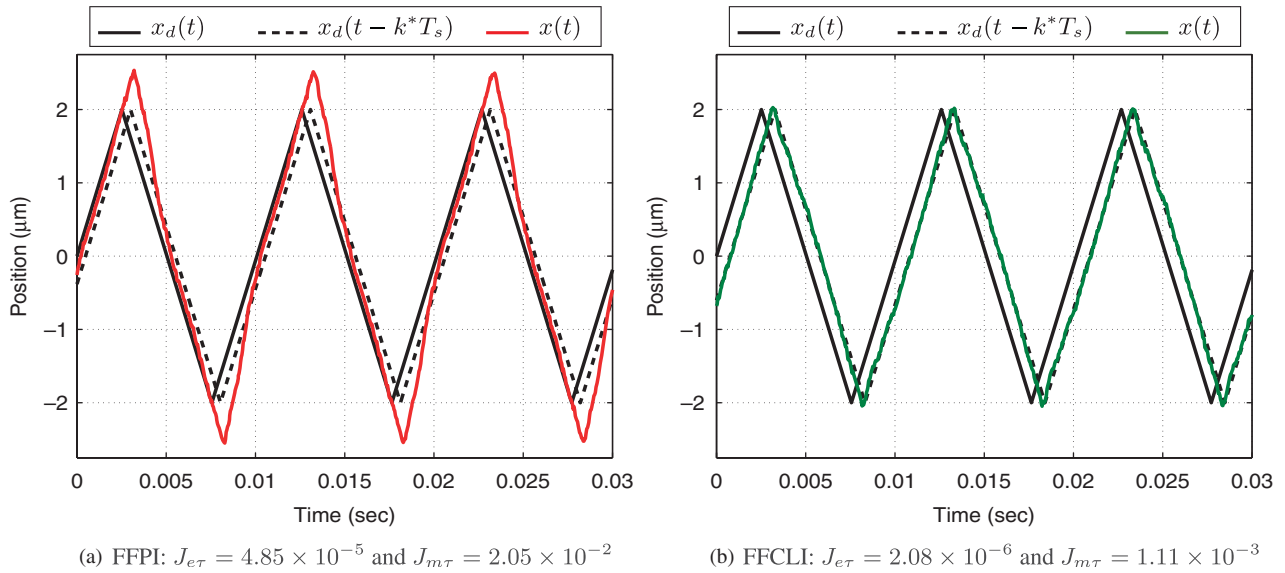


Fig. 3. Experimental results for (a) ZMETC plant-injection feedforward and (b) ZMETC closed-loop-injection feedforward control when given a 99.2 Hz raster pattern. Three curves appear in each figure: the $x_d(t)$ input, the $x_d(t - k * T_s)$ used for the performance metrics $J_{e\tau}$ and $J_{m\tau}$, and the $x(t)$ output. The metric values for each experiment are provided in the corresponding sub-captions.

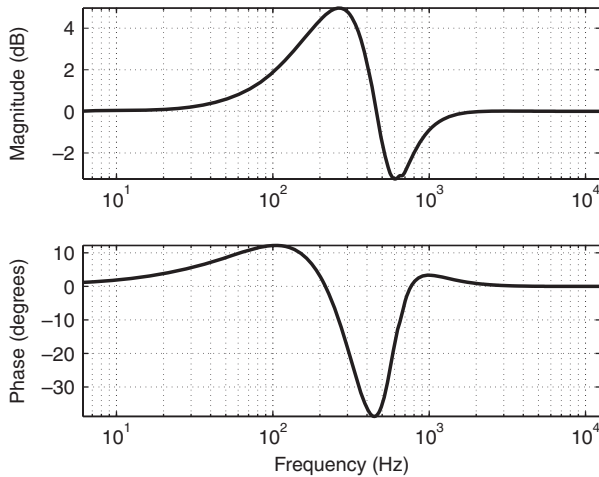


Fig. 4. The frequency response of the transfer function $\Psi(z)$ in (14) which is the factor that differentiates the two overall transfer functions for each architecture (equations (15) and (18)). This plot was created using the model for the plant P and the feedback controller C .

There is one key disadvantage to the FFCLI system. Specifically, F_{CL} can become a rather high-order filter in order to capture all the necessary inverse dynamics of the closed-loop system. This can be a problem for implementation, not only due to the high order, but also due to the numeric sensitivity that may result with such a high order.

Advanced control of AFMs is a growing area and there is much more work to be done and many areas to

be explored. Our future work will include refinement of our system identification techniques and a thorough investigation of how one might jointly design the feedforward and feedback compensators.

REFERENCES

1. Butterworth, J. A., L. Y. Pao, and D. Y. Abramovitch, "Architectures for tracking control in atomic force microscopes," *Proc. IFAC World Cong.*, Seoul, Korea, pp. 8236–8250 (2008).
2. Croft, D. and S. Devasia, "Vibration compensation for high speed scanning tunneling microscopy," *Rev. Sci. Instr.*, Vol. 70, No. 12, pp. 4600–4605 (1999).
3. Croft, D., G. Shedd, and S. Devasia, "Creep, hysteresis, and vibration compensation for piezoactuators: atomic force microscopy application," *ASME J. Dyn. Sys., Meas., & Control*, Vol. 123, pp. 35–43 (2001).
4. Schitter, G., R. W. Stark, and A. Stemmer, "Fast contact-mode atomic force microscopy on biological specimen by model-based control," *Ultramicroscopy*, Vol. 100, pp. 253–257 (2004).
5. Schitter, G. and A. Stemmer, "Identification and open-loop tracking control of a piezoelectric tube scanner for high-speed scanning-probe microscopy," *IEEE Trans. Control. Syst. Technol.*, Vol. 12, No. 3, pp. 449–454 (2004).

6. Tien, S., Q. Zou, and S. Devasia, "Iterative control of dynamics-coupling-caused errors in piezoscanners during high-speed AFM Operation," *IEEE Trans. Control Syst. Technol.*, Vol. 13, No. 6, pp. 921–931 (2005).
7. Devasia, S., "Review of feedforward approaches for nano precision positioning in high speed SPM operation," *Proc. IFAC World Cong.*, Seoul, Korea, pp. 9221–9229 (2008).
8. Devasia, S., E. Eleftheriou, and S. O. R. Moheimani, "A survey of control issues in nanopositioning," *IEEE Trans. Control Syst. Technol.*, Vol. 15, No. 5, pp. 802–823 (2007).
9. Li, Y. and J. Bechhoefer, "Feedforward control of a closed-loop piezoelectric translation stage for atomic force microscope," *Rev. Sci. Instrum.*, Vol. 78, pp. 013702-1-8 (2007).
10. Zou, Q. and S. Devasia, "Preview-based optimal inversion for output tracking: application to scanning tunneling microscopy," *IEEE Trans. Control Syst. Technol.*, Vol. 12, No. 3, pp. 375–386 (2004).
11. Rigney, B. P., L. Y. Pao, and D. A. Lawrence, "Nonminimum phase dynamic inversion for settle time applications," *IEEE Trans. Control Syst. Technol.*, Vol. 17, No. 3 (2009), in press.
12. Leang, K. K. and S. Devasia, "Feedback-linearized inverse feedforward for creep, hysteresis, and vibration compensation in AFM piezoactuators," *IEEE Trans. Control Syst. Technol.*, Vol. 15, No. 5, pp. 927–935 (2007).
13. Potsaid, B. and J. T. Wen, "High performance motion tracking control," *Proc. IEEE Int. Conf. Control Apps.*, Taipei, Taiwan, pp. 718–723 (2004).
14. Tomizuka, M., "Zero phase error tracking algorithm for digital control," *ASME J. Dyn. Syst., Meas., & Control*, Vol. 109, pp. 65–68 (1987).
15. Wen, J. T. and B. Potsaid, "An experimental study of a high performance motion control system," *Proc. Am. Control Conf.*, Boston, MA, U.S.A., pp. 5158–5163 (2004).
16. Butterworth, J. A., L. Y. Pao, and D. Y. Abramovitch, "The effect of nonminimum-phase zero locations on the performance of feedforward model-inverse control techniques in discrete-time systems," *Proc. Am. Control Conf.*, Seattle, WA, U.S.A., pp. 2696–2702 (2008).